Nano Energy 157 (2026) 112271

Contents lists available at ScienceDirect

Nano Energy

journal homepage: www.elsevier.com/locate/nanoen

Full paper

The biodegradable wireless constant-current stimulator

Luo Lin [a], Yongfang Ren [a], Tian Le [a], Engui Wang [a,b], Zhou Li [c,d], Han Ouyang [a,*]

[a] School of Nanoscience and Engineering, School of Chemical Sciences, University of Chinese Academy of Sciences, Beijing, China
[b] College of Materials Science and Opto-Electronic Technology, University of Chinese Academy of Sciences, Beijing, China
[c] Vita Tech Innovation Center, Tsinghua Changgung Hospital, School of Clinical Medicine, Tsinghua University, Beijing 100084, China
[d] School of Biomedical Engineering, Tsinghua Medicine, Beijing 100084, China

ARTICLE INFO

Keywords:
Biodegradable
Implantable electrical stimulator
Transient bioelectronics

ABSTRACT

Biodegradable electrical stimulators have emerged as a promising approach to temporary therapy. However, due to the absence of customizable biodegradable resistors, the clinically preferred constant-current stimulation remains unattainable. Dynamic impedance shifts caused by electrode degradation and tissue encapsulation can lead to unexpected stimulation outcomes in non-constant-current devices. Here, we present a highly stable biodegradable wireless constant-current stimulator based on customizable biodegradable resistors that suppresses output current fluctuations to $< 1.1\%$ across a typical impedance range of 0.5 kΩ to 2.6 kΩ. Its core electronic components are a customizable MXene/bacterial cellulose biodegradable resistor (1 kΩ–1 MΩ). Exploiting nonlinear volume expansion within the 1D/2D porous scaffold, we suppress the abrupt resistivity drop near the percolation threshold, thus mitigating the sharp transition typical of traditional composites. Ultimately, the wireless constant-current system integrating these customizable resistors ensures consistent therapy, should expand the clinical viability of next-generation transient electrophysiological therapeutics.

1. Introduction

Implantable electronic medical devices hold significant clinical value in regulating human physiological functions. In electrical stimulation therapy, constant-current stimulation ensures the consistency of neural recruitment and effectively prevents tissue damage, making it the current preferred clinical approach (Fig. 1a and b) [1–14]. However, constrained by the non-degradable nature of bio-inert materials, traditional devices typically require a secondary surgical removal after completing their temporary therapeutic tasks. This not only increases the risk of infection for patients but also imposes additional physiological burdens and medical expenses.

The emergence of biodegradable electrical stimulation devices offer an effective solution to eliminate the need for secondary surgeries. Upon completing the treatment, these devices can safely degrade in vivo through body fluid hydrolysis or metabolism. Currently, such devices typically rely on biodegradable metals (e.g., Mg, Mo) or polymers (e.g., PLGA, PLLA) as electrode interfaces [15–36]. However, in practical applications, influenced by dynamic factors such as the erosion of the electrode material itself, the infiltration of tissue exudate, and the growth of a fibrous capsule triggered by foreign body reactions, the interfacial impedance between the implanted device's electrode and the tissue experiences severe and uncontrollable fluctuations. This impedance instability directly causes the output current to deviate from preset values, subsequently leading to the attenuation or even failure of the therapeutic effect (Fig. 1c) [37–44].

To address this challenge, this study developed a highly stable, biodegradable, wireless constant-current electrical stimulator. The device is capable of outputting biomimetic spike signals and clinical electrical stimulation parameters ranging from 0 to 2 mA. The core of the research lies in utilizing MXene/BC composite materials to achieve the large-scale manufacturing of biodegradable resistors ranging from 1 kΩ to 1 MΩ. When the device internal resistance R_0 is much greater than the actual impedance at the stimulation site R_{load}, the stimulation current is primarily determined by R_0. Because R_0 is significantly larger than the fluctuation range of the interface impedance, the circuit's sensitivity to variations in load impedance is effectively reduced. (Fig. 1c and Figure S1, Supporting Information). Experimental results demonstrate that this strategy successfully controls the current fluctuation amplitude to below 5.2%. Lastly, in a rat model, by precisely regulating the magnitude of the stimulation current via a wireless mode, varying degrees of lower limb movements were successfully induced,

* Corresponding author.
E-mail address: ouyanghan@ucas.ac.cn (H. Ouyang).

https://doi.org/10.1016/j.nanoen.2026.112271
Received 26 May 2026; Received in revised form 4 August 2026; Accepted 4 August 2026
Available online 5 August 2026

fully validating the clinical potential and effectiveness of the device for precise motor control.

2. Result

2.1. Percolation threshold of MXene filler

In this study, high-aspect-ratio MXene nanosheets are employed as conductive fillers to induce significant steric hindrance within a bacterial cellulose (BC) nanofiber network, triggering a nonlinear macroscopic volume expansion within the percolation regime. This buffering effect enhances the fault tolerance of the fabrication process, allowing precise tuning of biodegradable resistor resistance values while supporting large-scale production [45,46]. The MXene/BC composite exhibits a percolation threshold of 6 wt% and a non-universal critical exponent of ($t = 2.7$) (Fig. 2a, and Figure S2, Supporting Information). This electrical behavior is closely related to three microstructural phases: at extremely low MXene loadings, the composite membrane maintains an initial dense-packing state dominated by the BC network. As the MXene content increases, the 2D nanosheets generate substantial steric hindrance within the 3D fiber network, constructing a porous scaffold that leads to a dramatic increase in film thickness; subsequently, at higher MXene loadings, van der Waals forces between the nanosheets drive their restacking, resulting in the collapse of the porous architecture and a subsequent regression in film thickness. (Fig. 2 b, c and Figure S3, Supporting Information).

In the XRD pattern, it can be observed that as the BC content increases, the interlayer spacing of MXene shifts from 1.27 nm to 1.46 nm (Figure S4a, Supporting Information). In the infrared spectrum, with the increase in BC content, the hydrogen bond network strengthens, and the infrared absorption peak of hydroxyl groups undergoes a red shift (Figure S4b, Supporting Information) (Fig. 2c).

2.2. Fabrication of biodegradable resistors

The integration of MXene thin film deposition technology with high-precision laser micromachining enables the large-scale manufacturing of resistors. In accordance with the E12 series standard for electronic components, we provide biodegradable resistors with an accuracy of ±10% (Fig. 3a). Based on this curve, five MXene thin films with different BC contents were selected, and standardized biodegradable resistors with resistance values ranging from 1 kΩ to 1 MΩ were fabricated to meet the requirements for modulating electrical stimulation current (Fig. 3c, and d). The amplitude-frequency characteristics from 0 to 100 kHz are measured, with minimal impedance fluctuations in the high-frequency range (Figure S5, Supporting Information). In long-term experiments in PBS at 37 °C, using the high-value resistor as a component ensures that the device can operate continuously for 72 h with a resistance fluctuation of less than 10% (Figure S6, Supporting Information).

2.3. Biodegradable wireless constant current electrical stimulator

The biomimetic spiking signals is wirelessly transmitted to the implanted device, and the pulse width can be adjusted through an external capacitor to meet stimulation requirements of less than 1 millisecond (Fig. 4a and Figure S7, Supporting Information). The implanted device can be paired with resistors exceeding 50 kΩ to provide a constant output current of less than 2 mA for the biomimetic spiking signals (Fig. 4c and d). In conventional electrical stimulation therapy, the

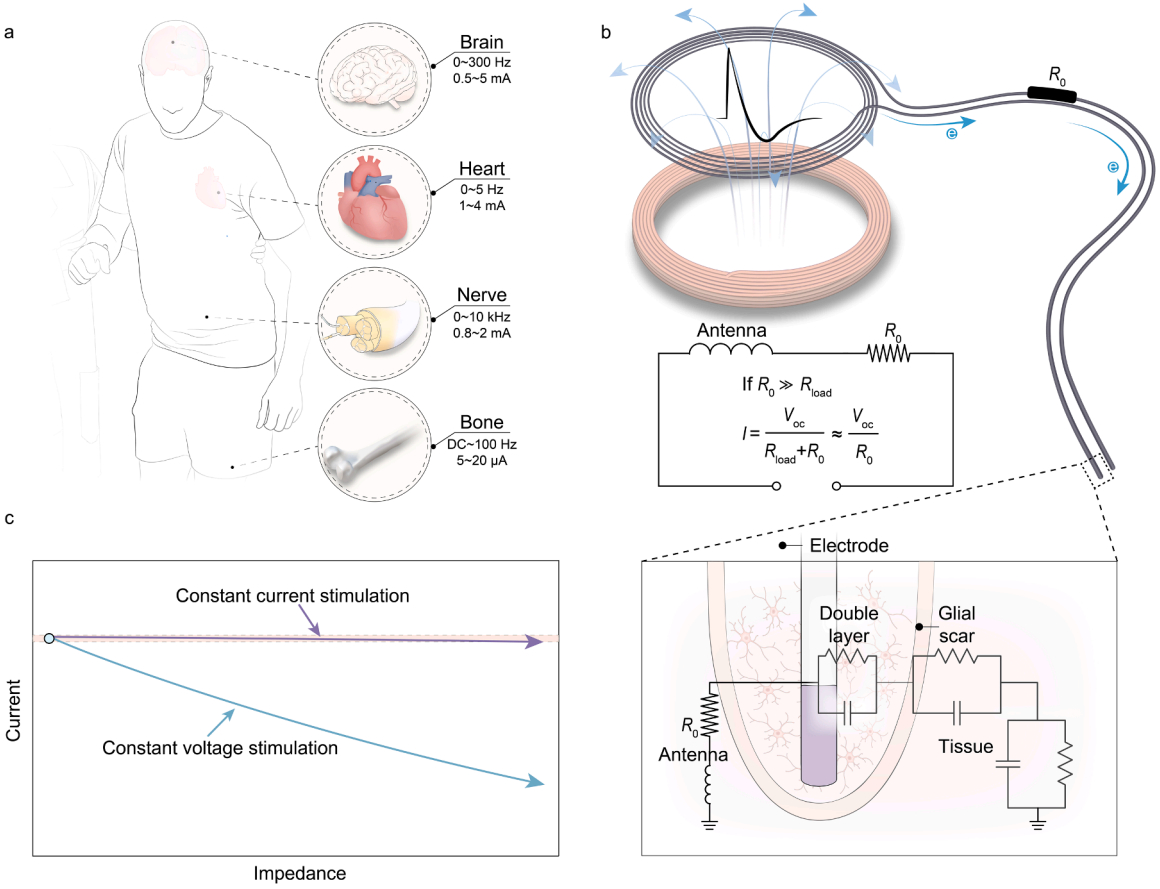

Fig. 1. Schematic diagram of a biodegradable constant current stimulator. a) Applications of Implantable Electrical Stimulation. b) Constant current electrical stimulation waveforms. c) Comparison of current fluctuations between constant-voltage electrical stimulation and constant-current electrical stimulation under impedance fluctuations. d) Schematic diagram of constant current electrical stimulation under bioimpedance fluctuations.

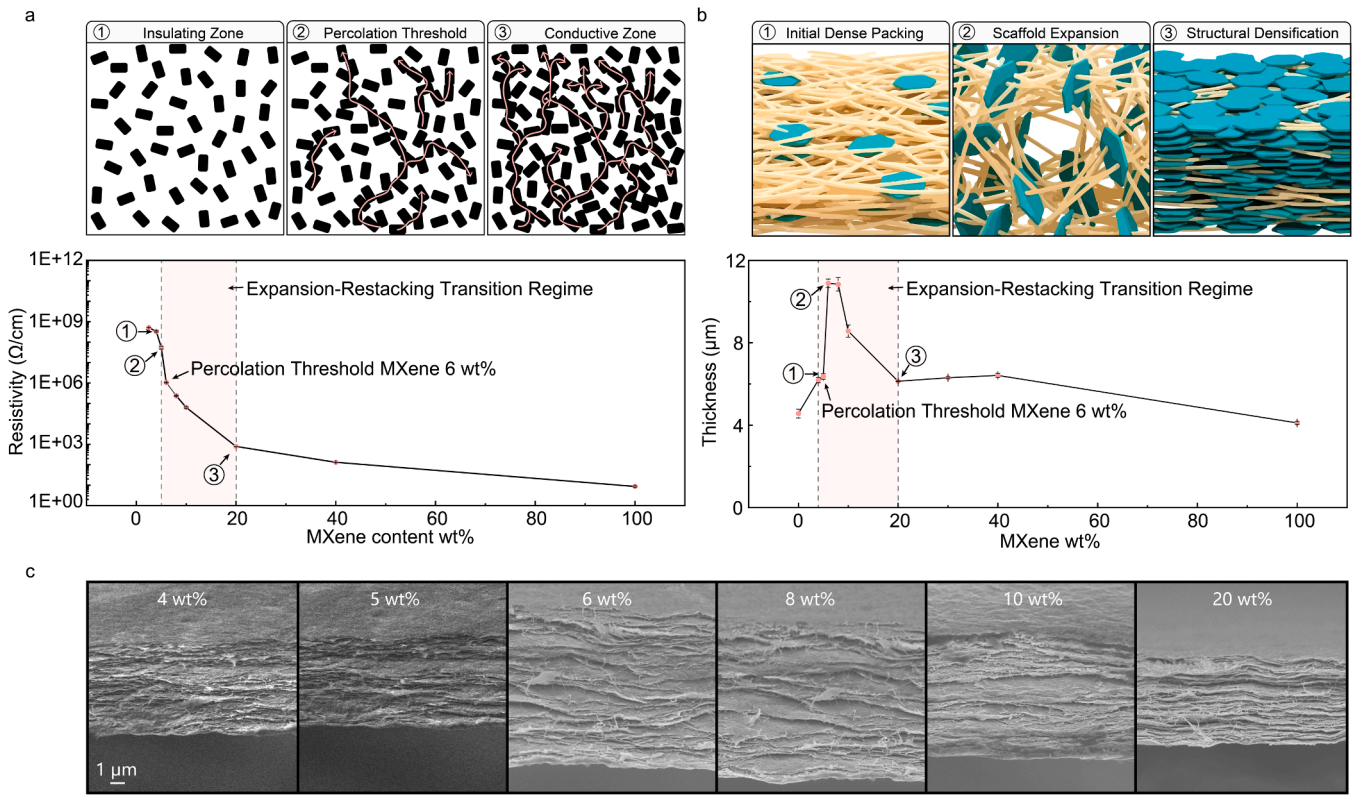

Fig. 2. Percolation threshold of MXene/BC composite material. a) The changes and attenuation of surface resistivity of MXene films with different MXene contents (n = 3). b) The changes of film thickness of films with different MXene contents (n = 3). c) SEM images of MXene/BC films with different ratios.

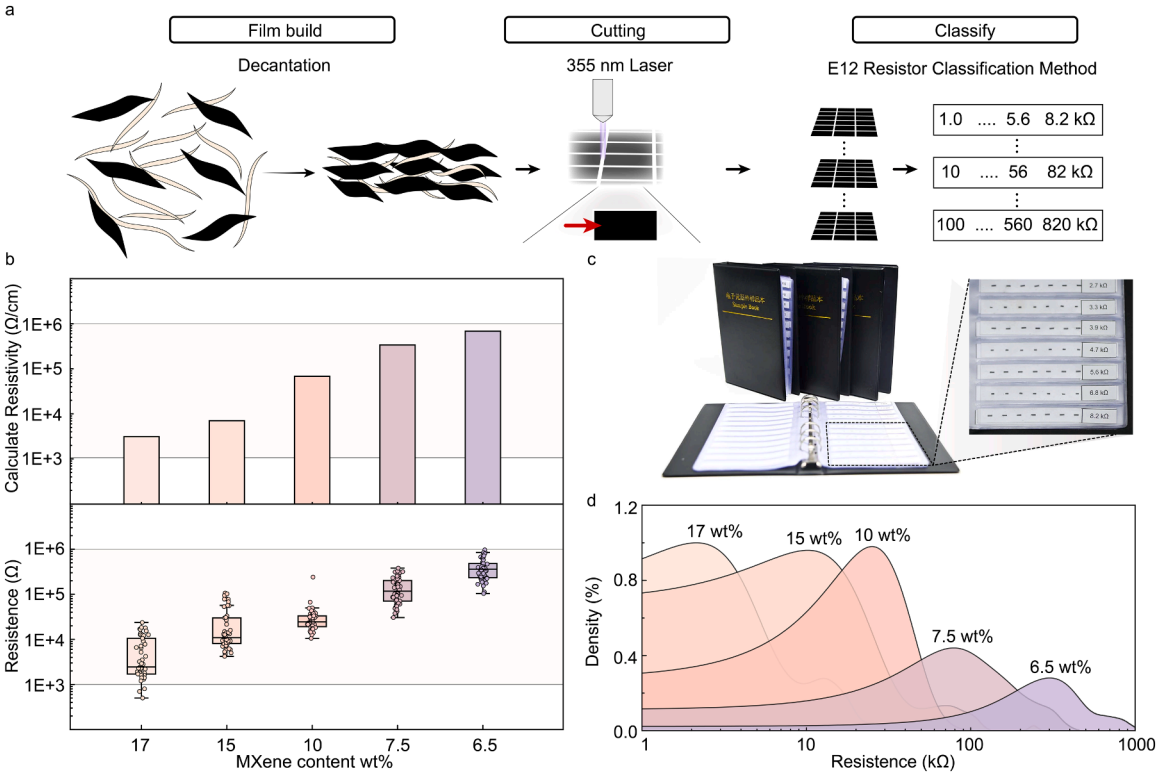

Fig. 3. Biodegradable resistance preparation. a) Schematic diagram and photos of the standardized preparation process of biodegradable resistance. b) Selection of different BC contents for the preparation of standardized resistors ranging from 1 kΩ to 1 MΩ (n = 50). c) Photo of E12 series standard resistors. d) Distribution map of biodegradable resistors fabricated from MXene films with five different BC contents (n = 50).

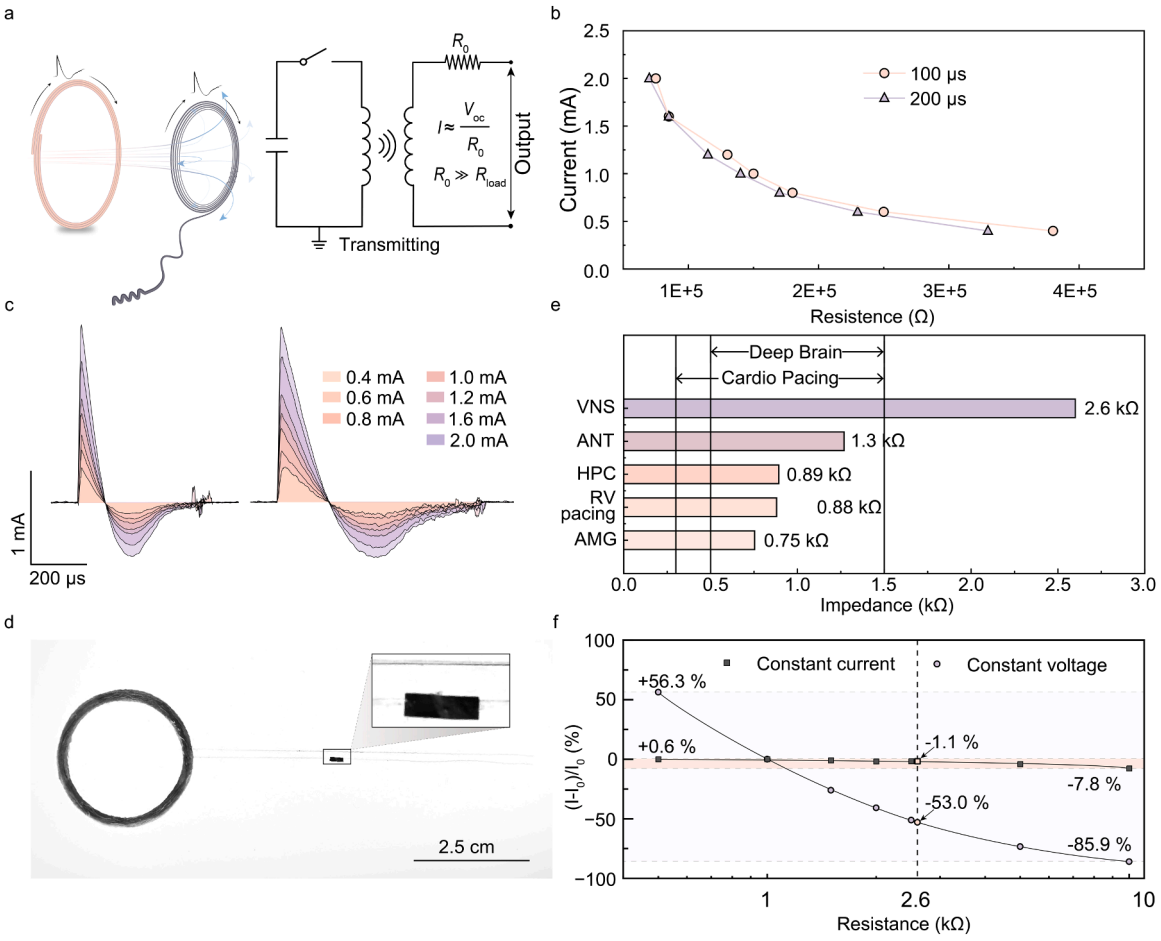

Fig. 4. Biomorphic spiking signals constant current output control. a) Schematic diagram of wireless constant-current electrical stimulation. b) Constant current output control for implantable devices. c) Relationship between constant current and internal resistance in implantable devices. d) Wireless constant-current stimulator photo and resistance magnification diagram. e) Range of electrical stimulation impedance changes in different body regions. f) Constant voltage electrical stimulation current fluctuation range.

impedance change typically remains below 2.6 kΩ [47–54]. Assuming a universal bioimpedance of 1 kΩ for electrical stimulation, the resulting variation in current due to changes in bioimpedance can be controlled to less than 1.1% (Fig. 4e and f). This ensures the stability and precision of the stimulation, maintaining effective therapeutic outcomes while minimizing any potential adverse effects. The ability to wirelessly transmit the signal and adjust the pulse width further enhances the flexibility of the system, enabling it to cater to a wide range of therapeutic needs.

2.4. *Wireless constant-current electrical stimulation of the sciatic nerve*

A constant-current stimulator for wireless biomimetic spiking signals can stimulate the sciatic nerve to control lower limb movement (Fig. 5a). The current intensity required for a 100 μs biomimetic spiking signals is significantly higher than that for a 200 μs signal, and it offers a wider window for adjustable current intensity. (Fig. 5b, c and d). When stimulating nerves with bionic spike signals of two pulse widths, increased current intensity leads to activation of more nerve fibers and muscle fibers, resulting in larger compound action potentials and greater oscillation amplitudes (Fig. 5e and f). This phenomenon illustrates how control over the pulse signal's duration. Moreover, it can effectively compensate for in vivo impedance fluctuations and maintain stable stimulation output, thereby achieving reliable modulation of the degree of neural and muscle activation.

2.5. *Cellular safety and biocompatibility of biodegradable resistors*

MXene resistors possess both degradability and biocompatibility, making them suitable for use in biomedical applications. Over a period of 37 days, the MXene resistors were gradually encapsulated by the surrounding tissue, with their volume steadily decreasing over the course of 76 days. Notably, during the degradation process, no significant encapsulation was observed, and there were no apparent inflammatory responses, suggesting that the degradation occurred in a controlled manner without triggering adverse tissue reactions (Fig. 6a, b, and c). Furthermore, when compared to the control group, cell cytoskeleton staining revealed no significant abnormalities, indicating that the presence of MXene resistors did not cause noticeable disruptions to cell structure or function (Fig. 6d and e).

3. Conclusion

The biodegradable wireless constant-current stimulator achieves precise regulation of the output current by integrating a high-resistance biodegradable resistor, enhancing the stability and reliability of electrical stimulation interventions. Simultaneously, the scalable fabrication strategy for this resistor provides a viable manufacturing solution for the mass production of transient electronic components. Although multi-component complex systems impose more stringent requirements on the long-term electrical stability of resorbable elements, future advancements are expected to further overcome the bottleneck in the

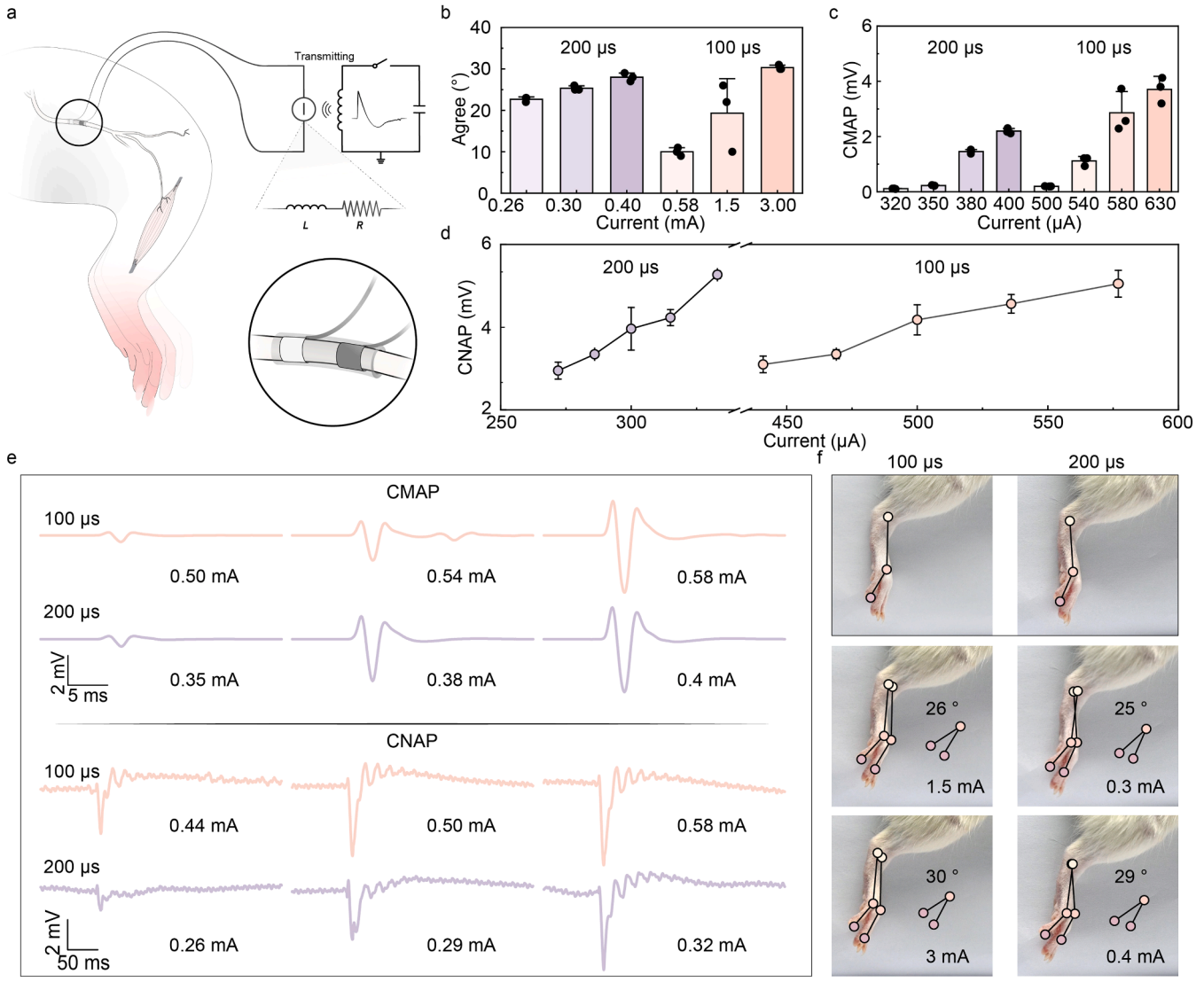

Fig. 5. Wireless constant-current electrical stimulation of the sciatic nerve. a) Schematic diagram of wireless constant-current electrical stimulation of the sciatic nerve) b) Angular variation under two different current intensities with varying pulse widths. c) Variation in maximum compound muscle action potential (CMAP) peak under two different current Intensities with distinct pulse widths. d) Variation in compound nerve action potential (CNAP) peak values at two different current intensities with distinct pulse widths. e) Changes in CMAP and CNAP waveforms at different current intensities. f) Photographs of foot swing angles at different current intensities.

system integration of biodegradable devices by synergistically optimizing the impedance matching of other electronic components within the circuit. Looking ahead, this highly stable biodegradable resistor can not only serve as an independent core impedance-regulating unit, but will also pave the way for broader application scenarios in the next generation of biodegradable neural stimulation and electrophysiological therapeutic devices.

4. Methods and materials

4.1. The MXene materials were prepared using the following method

(1) Etching: 5 mL of deionized (DI) water was added to 15 mL of 36%–38% HCl to prepare solution A Then, 1 g of LiF and 1 g of MAX phase (Ti_3AlC_2) were dissolved in solution A to obtain solution B, which was stirred at 40°C for 24 h. (2) 20 mL of solution B was mixed with 15 mL of DI water to prepare solution C Subsequently, solution C was centrifuged at 3500 rpm for 3 min. Then, discard the supernatant, rinse with 35 mL DI water and centrifuge again. Repeat this step until the pH value of the supernatant drops to 6.0, and the precipitate is obtained. (3) Finally, the precipitate was diluted with DI water and treated with ultrasound in an ice bath for 1 h. Then, it was centrifuged at 3500 rpm for 60 min to obtain a dispersed single-layer $Ti_3C_2T_x$ nanosheet.

The MXene/BC electrode was prepared by vacuum filtration of the mixed solution, which was obtained by thoroughly stirring MXene and BC in a 9:1 mass ratio.

4.2. Fabrication of biodegradable wires

Biodegradable wires were produced by subjecting Mo wires to a series of treatments, including electropolishing, zinc electroplating, and fusion encapsulation. The process began by cleaning 35 μm Mo wires using hydrochloric acid followed by deionized water. The Mo wire was then electropolished in a 10 wt% KOH solution until its diameter was reduced to 21 μm. The electropolishing was conducted at a current of 100 mA for a duration of 5 min. After rinsing the wire with deionized water, it was electroplated with zinc using a zinc solution, followed by another rinse with deionized water. The electroplating current was set at 10 mA, and the plating process lasted for 10 min. In the final step, PPDO (Regenovo, 2.0–3.0 dL/g) was heated to 170°C until it became molten.

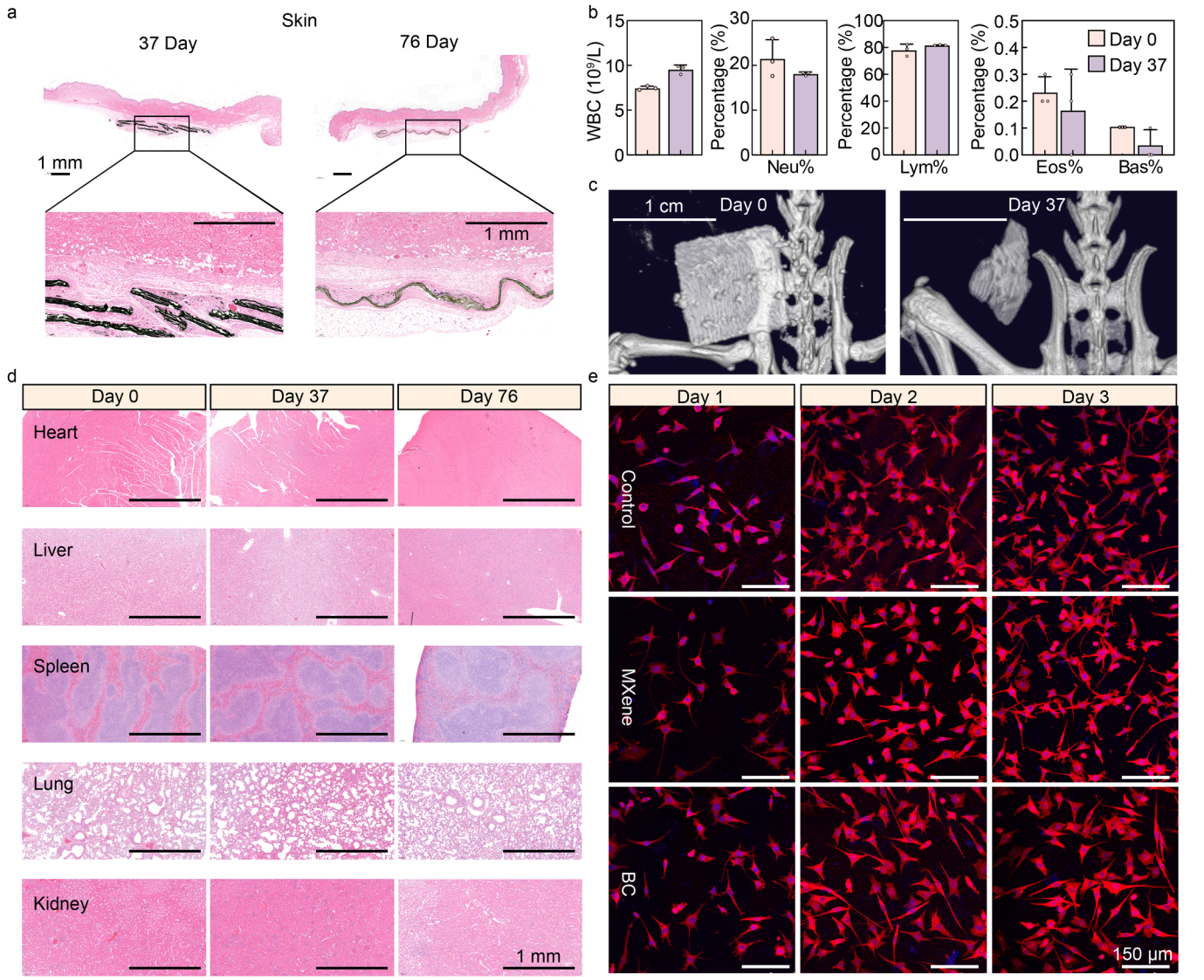

Fig. 6. Cellular safety and biocompatibility of biodegradable resistors. a) Tissue sections showing degradation of MXene films at 37 days and 76 days. b) Blood cell counts in MXene films degraded at 0 and 37 days. c) CT imaging of MXene film degradation at 0 days and 37 days. d) Effects of MXene film degradation at 0, 37, and 76 days on organ tissue sections. e) Cytoskeleton staining at 1, 2, 3 days (n = 3).

The zinc-coated Mo wire was then drawn through the molten PPDO and extruded through a nozzle with a 0.3 mm diameter, completing the fabrication of the biodegradable wire.

4.3. Fabrication of biodegradable monofiber device

The zinc-plated molybdenum wire, after passing through the molten PPDO, is quickly coiled around alumina ceramic rods with diameters of 10 mm or 25 mm. Once the winding is completed, the coils along with the reserved wire lengths are carefully removed and further encapsulated using a dichloromethane solution of PLGA (Sino-Tech Healthy, 75:25, 15 W, 15 wt%).

4.4. Characterization measurements

The morphology of the top surface, bottom surface, and cross-section of the MXene/BC films and related elemental information was characterized by scanning electron microscopy (SEM) (Regulus 8220). The chemical composition and state of FTIR was obtained using a VERTEX80v spectrometer (Bruker). Crystal and elementary compositions were analyzed by XRD, which was performed using PANalytical X'Pert3 Power with 2θ ranging from 5° to 10°, where Cu Kα radiation (λ = 1.5406 Å) was operated at 40 kV and 40 mA and Raman spectra were equipped with an Ar laser working at a wavelength of 532 nm (LabRAM HR Evolution, Horiba) at room temperature.

4.5. Wireless transmission experimental setup

The experimental setup for wireless transmission utilized a boost circuit (DC (12 V)-DC (500 V)) as the voltage source, which provided output to a transmitter circuit. This circuit included high-voltage capacitors (6.8, 10, 22, 33, 68 μF), discharge tubes (250, 300, 350 V), and inductors (0.64, 1.30, 1.87, 4.48 mH). The receiver section was composed of a 100-turn coil and lead wire made from 0.7 m of 110 μm insulated molybdenum wire) The open-circuit voltage (V_{oc}) was measured using an oscilloscope (Teledyne LeCroy WaveRunner 9104).

4.6. Cell culture

3T3 cells were cultured in DMEM medium (Solarbio), supplemented with 10% fetal bovine serum (FBS, Gibco) and 1% penicillin-streptomycin (Solarbio). The cells were incubated at 37°C in a 5% CO_2

atmosphere to maintain optimal growth conditions.

4.7. Cell morphology and cytoskeletal analysis

The effects of the four-material extract on cellular growth were further examined) Samples cultured in the exudate for 48 h were fixed at room temperature with 4% paraformaldehyde (Solarbio) for 10 min. After washing with PBS, the samples were permeabilized in 0.1% Triton X−100 (Solarbio) at 4°C for 5 min. They were washed again with PBS before being incubated with Rhodamine-podophyllotoxin (Abcam, diluted 1:1000) at 37°C for 1 h. Following another PBS wash, the samples were incubated with 4',6-diaminophenyl−2-indole (DAPI, Solarbio) for 10 min and then washed with PBS. The stained cells were subsequently observed under an ICX41 fluorescence microscope to visualize the cytoskeleton and nuclei.

4.8. In vivo degradation assessment

SD rats were allowed a one-week acclimatization period before undergoing surgery. The biodegradable monofiber device was sterilized by ultraviolet irradiation for one hour before being subcutaneously implanted in the dorsal region of the rats. Six months after implantation, the rats were euthanized, and histological analysis (H&E staining) was conducted on the tissues and organs surrounding the implanted antenna ($n = 3$). A complete blood count ($n = 3$) was performed using blood collected from the caudal vein into anticoagulant tubes. Inflammatory cell levels in the blood were analyzed using an animal hematology analyzer (52VET, Beijing Keyue Huacheng Technology).

4.9. Animal experiments

All rat experiments were performed according to protocols approved by the Committee on Ethics of the Beijing Institute of Nanoenergy and Nanosystems (2023016LZ), and all animal procedures were carried out in line with the national standards of the Laboratory Animal Requirements of Environment and Housing Facilities (GB14925–2001).

4.10. Statistical analysis

All experiments were repeated at least three times. Data were analyzed as mean ± standard deviation. Origin 2021 and GraphPad Prism version 8.0. were used for data analysis and plotting.

CRediT authorship contribution statement

Han Ouyang: Writing – review & editing, Resources, Funding acquisition, Conceptualization. **Luo Lin:** Writing – review & editing, Writing – original draft, Visualization, Formal analysis, Data curation, Conceptualization. **Engui Wang:** Resources, Funding acquisition, Formal analysis, Data curation, Conceptualization. **Zhou Li:** Writing – review & editing, Conceptualization. **Yongfang Ren:** Visualization, Formal analysis, Data curation. **Tian Le:** Visualization, Formal analysis, Data curation.

Funding

This work was supported by National Natural Science Foundation of China grants (52373256 to H.O.) and (62004010 to H.O.); National Key R&D project from Minister of Science and Technology, China (2023YFC2411901 to H.O.); Youth Innovation Promotion Association CAS (2023176 to H.O.); Supported by Beijing Natural Science Foundation (7232347 to H.O.) and (7264408 to E.W.); Beijing Nova Program grant 2024047 (to H.O.); Fundamental Research Funds for the Central Universities (to H.O.).

This work was also supported by the Synergetic Extreme Condition User Facility (SECUF, https://cstr.cn/31123.02.SECUF).

Declaration of Competing Interest

The authors declare that they have no known competing financial interests or personal relationships that could have appeared to influence the work reported in this paper.

Appendix A. Supporting information

Supplementary data associated with this article can be found in the online version at doi:10.1016/j.nanoen.2026.112271.

Data availability

No data was used for the research described in the article.

References

[1] J.M. Bronstein, M. Tagliati, C. McIntyre, R. Chen, T. Cheung, E.L. Hargreaves, Z. Israel, M. Moffitt, E.B. Montgomery, P. Stypulkowski, J. Shils, T. Denison, J. Vitek, J. Volkman, J. Wertheimer, M.S. Okun, The rationale driving the evolution of deep brain stimulation to constant-current devices, Neuromodulation Technol. Neural Interface 18 (2015) 85–89, https://doi.org/10.1111/ner.12227.

[2] S.F. Lempka, M.D. Johnson, S. Miocinovic, J.L. Vitek, C.C. McIntyre, Current-controlled deep brain stimulation reduces in vivo voltage fluctuations observed during voltage-controlled stimulation, Clin. Neurophysiol. 121 (2010) 2128–2133, https://doi.org/10.1016/j.clinph.2010.04.026.

[3] D.R. Merrill, M. Bikson, J.G.R. Jefferys, Electrical stimulation of excitable tissue: design of efficacious and safe protocols, J. Neurosci. Methods 141 (2005) 171–198, https://doi.org/10.1016/j.jneumeth.2004.10.020.

[4] H. Guan, Y. Tang, Z. Long, R. Lin, S. Liang, F. Zhu, T. Zhong, Y. Zhang, Y. Fan, Z. Wang, C. Shi, W. Ma, S. Sun, M. Chen, L. Xing, Y. Zhang, X. Xue, Y. Zhan, Cellphone remote intelligent neuroregulation with self-powered piezoelectric wireless brain probe, Nano Energy 106 (2023) 108105, https://doi.org/10.1016/j.nanoen.2022.108105.

[5] A.-H. Lee, J. Lee, V. Leung, L. Larson, A. Nurmikko, Patterned electrical brain stimulation by a wireless network of implantable microdevices, Nat. Commun. 15 (2024) 10093, https://doi.org/10.1038/s41467-024-54542-1.

[6] Y. Zeng, C. Gong, G. Lu, J. Wu, X. Wan, Y. Yang, J. Ji, J. Zhang, R. Li, Y. Sun, Z. Che, C.-F. Chang, H.-C. Liu, J. Chen, Q. He, X. Sun, R. Chen, S.K. Nejad, X. Liu, D. S. Rajendran Nair, L. Jiang, J. Chen, Q. Zhou, A programmable and self-adaptive ultrasonic wireless implant for personalized chronic pain management, Nat. Electron. 8 (2025) 437–449, https://doi.org/10.1038/s41928-025-01374-6.

[7] T. Zhong, H. Yi, J. Gou, J. Li, M. Liu, X. Gao, S. Chen, H. Guan, S. Liang, Q. He, R. Lin, Z. Long, Y. Wang, C. Shi, Y. Zhan, Y. Zhang, L. Xing, J. Zhong, X. Xue, A wireless battery-free eye modulation patch for high myopia therapy, Nat. Commun. 15 (2024) 1766, https://doi.org/10.1038/s41467-024-46049-6.

[8] P. Zou, R. Lin, Z. Fang, J. Chen, H. Guan, J. Yin, Z. Chang, L. Xing, J. Lang, X. Xue, M. Chen, Implanted, wireless, self-powered photodynamic therapeutic tablet synergizes with ferroptosis inducer for effective cancer treatment, Adv. Sci. 10 (2023) 2302731, https://doi.org/10.1002/advs.202302731.

[9] W. Wang, M. Sun, Z. Zhang, S. Guo, H. Sun, Z. Wei, B. Ning, Application of microenvironment biomimetic materials in spinal cord injury and future prospects, Med. Mat. 2 (2025).

[10] J.-H. Zhang, J. Zhang, X. Zhang, X. Wang, Z. Zhang, X. Sun, H. Wang, Z. Liu, N. Sun, L. Pan, Three-dimensionally microarchitected electrospun fabric-enabled pressure-sensitive bioelectronics, Med. Mat. 3 (2026).

[11] H. Song, M. Kim, E. Kim, J. Lee, I. Jeong, K. Lim, S.Y. Ryu, M. Oh, Y. Kim, J.-U. Park, Neuromodulation of the peripheral nervous system: bioelectronic technology and prospective developments, BMEMat 2 (2024) e12048, https://doi.org/10.1002/bmm2.12048.

[12] H. Wang, H. Wu, D. Ye, C. Zhao, Q. Wu, S. Wang, Z. Zhang, M. Zeng, H. Wei, Y. Huang, Micro-cylindrical/fibric electronic devices: materials, fabrication, health and environmental monitoring, Soft Sci. 4 (2024) 41, https://doi.org/10.20517/ss.2024.53.

[13] H. Ouyang, Z. Liu, N. Li, B. Shi, Y. Zou, F. Xie, Y. Ma, Z. Li, H. Li, Q. Zheng, X. Qu, Y. Fan, Z.L. Wang, H. Zhang, Z. Li, Symbiotic cardiac pacemaker, Nat. Commun. 10 (2019) 1821, https://doi.org/10.1038/s41467-019-09851-1.

[14] H. Ouyang, D. Jiang, Y. Hu, S. Cheng, Z. Zhang, B. Shi, E. Wang, J. Xue, Y. Shan, L. Xu, Y. Zou, S. Weng, H. Li, H. Niu, M. Gu, L. Luo, S. Chao, P. Tan, Y. Yao, N. Wang, Y. Fan, Z.L. Wang, W. Hua, Z. Li, Symbiotic transcatheter pacemaker for lifelong energy regeneration and therapeutic function in porcine disease model, Nat. Biomed. Eng. (2026), https://doi.org/10.1038/s41551-025-01604-4.

[15] Y.-J. Kim, S.-H. Kim, B.-J. Park, J. Jeon, D. Kang, Y. Chung, J.-H. Hwang, H.-J. Yoon, K.H. Lee, B.-O. Choi, S.-W. Kim, Wireless and bioresorbable triboelectric nerve block system for postoperative pain control, Nat. Biomed. Eng. (2026), https://doi.org/10.1038/s41551-025-01579-2.

[16] G. Lee, E. Ray, H.-J. Yoon, S. Genovese, Y.S. Choi, M.-K. Lee, S. Şahin, Y. Yan, H.-Y. Ahn, A.J. Bandodkar, J. Kim, M. Park, H. Ryu, S.S. Kwak, Y.H. Jung, A. Odabas, U. Khandpur, W.Z. Ray, M.R. MacEwan, J.A. Rogers, A bioresorbable peripheral nerve stimulator for electronic pain block, Sci. Adv. 8 (2026) eabp9169, https://doi.org/10.1126/sciadv.abp9169.

[17] Y.S. Choi, R.T. Yin, A. Pfenniger, J. Koo, R. Avila, K. Benjamin Lee, S.W. Chen, G. Lee, G. Li, Y. Qiao, A. Murillo-Berlioz, A. Kiss, S. Han, S.M. Lee, C. Li, Z. Xie, Y.-Y. Chen, A. Burrell, B. Geist, H. Jeong, J. Kim, H.-J. Yoon, A. Banks, S.-K. Kang, Z. J. Zhang, C.R. Haney, A.V. Sahakian, D. Johnson, T. Efimova, Y. Huang, G. D. Trachiotis, B.P. Knight, R.K. Arora, I.R. Efimov, J.A. Rogers, Fully implantable and bioresorbable cardiac pacemakers without leads or batteries, Nat. Biotechnol. 39 (2021) 1228–1238, https://doi.org/10.1038/s41587-021-00948-x.

[18] P. Liu, L. Zhou, D. Xu, D. An, Y. Lu, B. Hu, Y. Shao, N. Huang, C. Guo, L. Chen, J. Li, J. Li, F. Liang, J. Liu, G. Huang, Y. Mei, R. Li, E. Song, A self-wrapping, bioresorbable neural interface for wireless multimodal therapy of localized peripheral nerve injury, Proc. Natl. Acad. Sci. 123 (2026) e2521817123, https://doi.org/10.1073/pnas.2521817123.

[19] J. Koo, M.R. MacEwan, S.-K. Kang, S.M. Won, M. Stephen, P. Gamble, Z. Xie, Y. Yan, Y.-Y. Chen, J. Shin, N. Birenbaum, S. Chung, S.B. Kim, J. Khalifeh, D. V. Harburg, K. Bean, M. Paskett, J. Kim, Z.S. Zohny, S.M. Lee, R. Zhang, K. Luo, B. Ji, A. Banks, H.M. Lee, Y. Huang, W.Z. Ray, J.A. Rogers, Wireless bioresorbable electronic system enables sustained nonpharmacological neuroregenerative therapy, Nat. Med. 24 (2018) 1830–1836, https://doi.org/10.1038/s41591-018-0196-2.

[20] H.-Y. Ahn, J.B. Walters, R. Avila, S. Oh, S.G. Seo, J.U. Kim, J. Park, S. Yoo, Y. S. Choi, T.Y. Kim, J. Liu, J.-Y. Yoo, O.R. Weissleder, D. D'Andrea, C. Park, G. Lee, D. Cho, W.-Y. Maeng, H.-J. Yoon, G. Wickerson, Y. Bouricha, J. Tian, T.C. Chung, S. W. Jordan, S. Li, Y. Huang, C.K. Franz, J.A. Rogers, Bioresorbable, wireless dual stimulator for peripheral nerve regeneration, Nat. Commun. 16 (2025) 4752, https://doi.org/10.1038/s41467-025-59835-7.

[21] L. Wang, C. Lu, S. Yang, P. Sun, Y. Wang, Y. Guan, S. Liu, D. Cheng, H. Meng, Q. Wang, J. He, H. Hou, H. Li, W. Lu, Y. Zhao, J. Wang, Y. Zhu, Y. Li, D. Luo, T. Li, H. Chen, S. Wang, X. Sheng, W. Xiong, X. Wang, J. Peng, L. Yin, A fully biodegradable and self-electrified device for neuroregenerative medicine, Sci. Adv. 6 (2020) eabc6686, https://doi.org/10.1126/sciadv.abc6686.

[22] Y. Zhang, E. Rytkin, L. Zeng, J.U. Kim, L. Tang, H. Zhang, A. Mikhailov, K. Zhao, Y. Wang, L. Ding, X. Lu, A. Lantsova, E. Aprea, G. Jiang, S. Li, S.G. Seo, T. Wang, J. Wang, J. Liu, J. Gu, F. Liu, K. Bailey, Y.F.L. Li, A. Burrell, A. Pfenniger, A. Ardashev, T. Yang, N. Liu, Z. Lv, N.S. Purwanto, Y. Ying, Y. Lu, C. Hoepfner, A. Melisova, J. Gong, J. Jeong, J. Choi, A. Hou, R. Nolander, W. Bai, S.H. Jin, Z. Ma, J.M. Torkelson, Y. Huang, W. Ouyang, R.K. Arora, I.R. Efimov, J.A. Rogers, Millimetre-scale bioresorbable optoelectronic systems for electrotherapy, Nature 640 (2025) 77–86, https://doi.org/10.1038/s41586-025-08726-4.

[23] Y. Huang, Y. Cui, H. Deng, J. Wang, R. Hong, S. Hu, H. Hou, Y. Dong, H. Wang, J. Chen, L. Li, Y. Xie, P. Sun, X. Fu, L. Yin, W. Xiong, S.-H. Shi, M. Luo, S. Wang, X. Li, X. Sheng, Bioresorbable thin-film silicon diodes for the optoelectronic excitation and inhibition of neural activities, Nat. Biomed. Eng. 7 (2023) 486–498, https://doi.org/10.1038/s41551-022-00931-0.

[24] P. Sun, C. Li, C. Yang, M. Sun, H. Hou, Y. Guan, J. Chen, S. Liu, K. Chen, Y. Ma, Y. Huang, X. Li, H. Wang, L. Wang, S. Chen, H. Cheng, W. Xiong, X. Sheng, M. Zhang, J. Peng, S. Wang, Y. Wang, L. Yin, A biodegradable and flexible neural interface for transdermal optoelectronic modulation and regeneration of peripheral nerves, Nat. Commun. 15 (2024) 4721, https://doi.org/10.1038/s41467-024-49166-4.

[25] Y.S. Choi, H. Jeong, R.T. Yin, R. Avila, A. Pfenniger, J. Yoo, J.Y. Lee, A. Tzavelis, Y. J. Lee, S.W. Chen, H.S. Knight, S. Kim, H.-Y. Ahn, G. Wickerson, A. Vázquez-Guardado, E. Higbee-Dempsey, B.A. Russo, M.A. Napolitano, T.J. Holleran, L. A. Razzak, A.N. Miniovich, G. Lee, B. Geist, B. Kim, S. Han, J.A. Brennan, K. Aras, S. S. Kwak, J. Kim, E.A. Waters, X. Yang, A. Burrell, K. San Chun, C. Liu, C. Wu, A. Y. Rwei, A.N. Spann, A. Banks, D. Johnson, Z.J. Zhang, C.R. Haney, S.H. Jin, A. V. Sahakian, Y. Huang, G.D. Trachiotis, B.P. Knight, R.K. Arora, I.R. Efimov, J. A. Rogers, A transient, closed-loop network of wireless, body-integrated devices for autonomous electrotherapy, Science 376 (2022) 1006–1012, https://doi.org/10.1126/science.abm1703.

[26] D.-M. Lee, M. Kang, I. Hyun, B.-J. Park, H.J. Kim, S.H. Nam, H.-J. Yoon, H. Ryu, H.-m Park, B.-O. Choi, S.-W. Kim, An on-demand bioresorbable neurostimulator, Nat. Commun. 14 (2023) 7315, https://doi.org/10.1038/s41467-023-42791-5.

[27] S.M. McDonald, Q. Yang, Y.-H. Hsu, S.P. Nikam, Z. Hu, Z. Wang, D. Asheghali, T. Yen, A.V. Dobrynin, J.A. Rogers, M.L. Becker, Resorbable barrier polymers for flexible bioelectronics, Nat. Commun. 14 (2023) 7299, https://doi.org/10.1038/s41467-023-42775-5.

[28] S.-W. Hwang, J.-K. Song, X. Huang, H. Cheng, S.-K. Kang, B.H. Kim, J.-H. Kim, S. Yu, Y. Huang, J.A. Rogers, High-performance biodegradable/transient electronics on biodegradable polymers, Adv. Mater. 26 (2014) 3905–3911, https://doi.org/10.1002/adma.201306050.

[29] L. Yin, H. Cheng, S. Mao, R. Haasch, Y. Liu, X. Xie, S.-W. Hwang, H. Jain, S.-K. Kang, Y. Su, R. Li, Y. Huang, J.A. Rogers, Dissolvable metals for transient electronics, Adv. Funct. Mater. 24 (2014) 645–658, https://doi.org/10.1002/adfm.201301847.

[30] S.-W. Hwang, H. Tao, D.-H. Kim, H. Cheng, J.-K. Song, E. Rill, M.A. Brenckle, B. Panilaitis, S.M. Won, Y.-S. Kim, Y.M. Song, K.J. Yu, A. Ameen, R. Li, Y. Su, M. Yang, D.L. Kaplan, M.R. Zakin, M.J. Slepian, Y. Huang, F.G. Omenetto, J. A. Rogers, A physically transient form of silicon electronics, Science 337 (2012) 1640–1644, https://doi.org/10.1126/science.1226325.

[31] S.-K. Kang, R.K.J. Murphy, S.-W. Hwang, S.M. Lee, D.V. Harburg, N.A. Krueger, J. Shin, P. Gamble, H. Cheng, S. Yu, Z. Liu, J.G. McCall, M. Stephen, H. Ying, J. Kim, G. Park, R.C. Webb, C.H. Lee, S. Chung, D.S. Wie, A.D. Gujar, B. Vemulapalli, A.H. Kim, K.-M. Lee, J. Cheng, Y. Huang, S.H. Lee, P.V. Braun, W. Z. Ray, J.A. Rogers, Bioresorbable silicon electronic sensors for the brain, Nature 530 (2016) 71–76, https://doi.org/10.1038/nature16492.

[32] Y. Bai, H. Meng, Z. Li, Z.L. Wang, Degradable piezoelectric biomaterials for medical applications, Med. Mat. 1 (2024).

[33] J. Hao, N.A.N.N. Malek, W.H.A. Kamaruddin, J. Li, Breaking piezoelectric limits of molecules for biodegradable implants, BMEMat 2 (2024) e12087, https://doi.org/10.1002/bmm2.12087.

[34] J. Zhang, Z. Shang, Y. Jiang, K. Zhang, X. Li, M. Ma, Y. Li, B. Ma, Biodegradable metals for bone fracture repair in animal models: a systematic review, Regen. Biomater. 8 (2021) rbaa047, https://doi.org/10.1093/rb/rbaa047.

[35] W. Ding, Opportunities and challenges for the biodegradable magnesium alloys as next-generation biomaterials, Regen. Biomater. 3 (2016) 79–86, https://doi.org/10.1093/rb/rbw003.

[36] Y.-J. Park, Y.-I. Ryu, M.-K. Choi, K.-S. Kim, S.-K. Kang, Controlling the lifetime of biodegradable electronics: from dissolution kinetics to trigger acceleration, Soft Sci. 4 (2024) 16, https://doi.org/10.20517/ss.2024.06.

[37] H.T. Nguyen, S. Sapp, C. Wei, J.K. Chow, A. Nguyen, J. Coursen, S. Luebben, E. Chang, R. Ross, C.E. Schmidt, Electric field stimulation through a biodegradable polypyrrole-co-polycaprolactone substrate enhances neural cell growth, J. Biomed. Mater. Res. A 102 (2014) 2554–2564, https://doi.org/10.1002/jbm.a.34925.

[38] S.M. Wellman, T.D.Y. Kozai, Understanding the inflammatory tissue reaction to brain implants to improve neurochemical sensing performance, ACS Chem. Neurosci. 8 (2017) 2578–2582, https://doi.org/10.1021/acschemneuro.7b00403.

[39] S. Carcieri, M. Reich, F. Steigerwald, M. Barbe, L. Manola, L. Timmermann, J. Volkmann, Impedance changes occur during threshold measurements in deep brain stimulation patients (P7.046), Neurology 82 (2014) P7.046, https://doi.org/10.1212/WNL.82.10_supplement.P7.046.

[40] C. Newbold, S. Mergen, R. Richardson, P. Seligman, R. Millard, R. Cowan, R. Shepherd, Impedance changes in chronically implanted and stimulated cochlear implant electrodes, Cochlea-.-. Implants Int. 15 (2014) 191–199, https://doi.org/10.1179/1754762813Y.0000000050.

[41] D. Satzer, D. Lanctin, L.E. Eberly, A. Abosch, Variation in deep brain stimulation electrode impedance over years following electrode implantation, Stereotact. Funct. Neurosurg. 92 (2014) 94–102, https://doi.org/10.1159/000358014.

[42] K.A. Sillay, P. Rutecki, K. Cicora, G. Worrell, J. Drazkowski, J.J. Shih, A.D. Sharan, M.J. Morrell, J. Williams, B. Wingeier, Long-term measurement of impedance in chronically implanted depth and subdural electrodes during responsive neurostimulation in humans, Brain Stimul. 6 (2013) 718–726, https://doi.org/10.1016/j.brs.2013.02.001.

[43] C. Newbold, R. Richardson, R. Millard, P. Seligman, R. Cowan, R. Shepherd, Electrical stimulation causes rapid changes in electrode impedance of cell-covered electrodes, J. Neural Eng. 8 (2011) 036029, https://doi.org/10.1088/1741-2560/8/3/036029.

[44] M. Corsi, E. Bellotti, S. Surdo, G. Barillaro, Implantable bioresorbable electronic systems for sustainable precision medicine, Nat. Rev. Electr. Eng. 2 (2025) 572–583, https://doi.org/10.1038/s44287-025-00190-6.

[45] D.S. McLachlan, M. Blaszkiewicz, R.E. Newnham, Electrical Resistivity of Composites, J. Am. Ceram. Soc. 73 (1990) 2187–2203, https://doi.org/10.1111/j.1151-2916.1990.tb07576.x.

[46] K. Dai, X. Wang, F. Yi, Y. Yin, C. Jiang, S. Niu, Q. Li, Z. You, Discharge voltage behavior of electric double-layer capacitors during high-g impact and their application to autonomously sensing high-g accelerometers, Nano Res. 11 (2018) 1146–1156, https://doi.org/10.1007/s12274-017-1740-y.

[47] A. Vydyanathan, B. Kosharskyy, S. Nair, K. Gritsenko, R.S. Kim, D. Wang, N. Shaparin, The use of electrical impedance to identify intraneural needle placement in human peripheral nerves: a study on amputated human limbs, Anesth. Analg. 123 (2016).

[48] A. Cukiert, C. Cukiert, R.B. Guimaraes, J.A. Burattini, J.V. Vieira, J.P.S. de Oliveira, Vagus nerve stimulation electrode impedance over time in children with lennox-gastaut syndrome, Neuromodulation 27 (2024) 789–791, https://doi.org/10.1016/j.neurom.2023.06.006.

[49] C.R. Butson, C.B. Maks, C.C. McIntyre, Sources and effects of electrode impedance during deep brain stimulation, Clin. Neurophysiol. 117 (2006) 447–454, https://doi.org/10.1016/j.clinph.2005.10.007.

[50] C.D. Swerdlow, J.N. Koneru, B. Gunderson, M.W. Kroll, S. Ploux, K.A. Ellenbogen, Impedance in the diagnosis of lead malfunction, Circulation Arrhythmia Electrophysiology 13 (2020) e008092, https://doi.org/10.1161/CIRCEP.119.008092.

[51] E. Nakagawa, Y. Abe, R. Komatsu, T. Naruko, A. Itoh, Right coronary artery perforation by an active-fixation atrial pacing lead resulting in life-threatening tamponade, J. Arrhythmia 31 (2015) 313–315, https://doi.org/10.1016/j.joa.2015.01.002.

[52] N. Sperelakis, T. Hoshiko, Electrical impedance of cardiac muscle, Circ. Res. 9 (1961) 1280–1283, https://doi.org/10.1161/01.RES.9.6.1280.

[53] J. Cinca, M. Warren, A. Carreño, M. Tresànchez, L. Armadans, P. Gómez, J. Soler-Soler, Changes in myocardial electrical impedance induced by coronary artery occlusion in pigs with and without preconditioning, Circulation 96 (1997) 3079–3086, https://doi.org/10.1161/01.CIR.96.9.3079.

[54] A. Fabregas, S. McKellar, S. Rutkove, R. Mandeville, B. Sanchez, Assessment of peripheral nerve injury with impedance neurography: a pilot in silico study, J. Phys. Conf. Ser. 3014 (2025) 012001, https://doi.org/10.1088/1742-6596/3014/1/012001.